CrystEngComm

Synthesis of Zirconium-Based Metal-Organic Frameworks with Iron(II) Clathrochelate Ligands

Journal:	*CrystEngComm*
Manuscript ID	CE-ART-12-2022-001686.R1
Article Type:	Paper
Date Submitted by the Author:	25-Jan-2023
Complete List of Authors:	Shetty, Suchetha; Gulf University for Science & Technology, Department of Mathematics and Natural Sciences Idrees, Karam; Northwestern University, Department of Chemistry Xie, Haomiao; Northwestern University Alameddine, Bassam; Gulf University for Science and Technology, Department of Mathematics and Natural Sciences Farha, Omar K. ; Northwestern University, Department of Chemistry and International Institute of Nanotechnology and Chemical and Biological Engineering

ARTICLE

Synthesis of Zirconium-Based Metal-Organic Frameworks with Iron(II) Clathrochelate Ligands

Received 00th January 20xx,
Accepted 00th January 20xx

DOI: 10.1039/x0xx00000x

Suchetha Shetty,[a,b,⊥] Karam B. Idrees,[c,⊥] Haomiao Xie,[c] Bassam Alameddine,[a,b,*] and Omar K. Farha[c,d,*]

Zirconium-based metal organic frameworks (MOFs) are of great significance in supramolecular coordination chemistry, mainly as catalysts, due to their chemical stability and structural diversity. We report the synthesis of Zirconium-clathrochelate based crystalline MOFs (Zr-GU-1 to -4) made from hexanuclear zirconium inorganic nodes and Iron (II) clathrochelate-based ditopic carboxylic acid ligands bearing various lateral moieties, namely, butyl, cyclohexyl, phenyl and methyl groups. Among the various iron (II) clathrochelate linkers, the one with butyl side chains i.e., Zr-GU-1 forms stable crystalline MOFs as confirmed by single-crystal X-ray crystallography and which exhibits a promising porosity with BET surface area of ~650 m^2 g^{-1} after its activation with supercritical CO_2 ($ScCO_2$) from acetonitrile.

Introduction

Metal-organic frameworks (MOFs) are constructed from inorganic metal ions/metal clusters and organic ligands which are linked together by coordination bonds to form a well-defined framework in both composition and structure[1,2]. Over the past few decades, the construction of metal-organic frameworks (MOFs) was among the most promising and rapidly expanding fields in materials science due to the unique properties that they disclose, namely, their bottom-up synthesis which allows for making on-demand structures, excellent flexibility, and porous nature whose large specific surface bearing active sites can be adjusted[3-5]. With these unique properties, MOFs have found a myriad of applications across different fields, such as, gas adsorption and separation[6-8], chemical sensing[9,10], catalysis[11,12], lithium-ion batteries[13,14], water treatment and biomedicine[15,16]. Recently, the preparation of MOFs has undergone a noticeable development by using multidentate aromatic carboxylic acid ligands as building blocks, due to their robustness and thermal stability[17,18]. Furthermore, these multidentate ligands can be easily deprotonated to balance the metal ion charge, without the need to include in the resulting framework lattice any additional uncoordinated counter-ions which would occupy the channel voids, and consequently, block the MOFs pores[19]. These characteristics of the metal-carboxylate lattices are utilized in size- and shape-selective separations and catalysis[20].

Reticular chemistry, whose rules allow for a rational design of MOFs to a great extent, has emerged as a powerful synthetic tool to alter the chemical composition, framework topology, porosity and its environment in porous crystalline materials[21-23]. By rationally choosing the target topologies and molecular building blocks, specific MOFs can be constructed with atomic precision[24,25]. Over the last few years, Zr-based MOFs have attracted a great attention due to their exceptional chemical stability[26-33] besides the applications of these materials in various fields, among others, their use as catalysts for organic syntheses[34-36] and hydrolytic decontaminants of chemical warfare agents[37-41]. Herein, we report the synthesis of Zr-based MOFs employing octahedral iron (II) clathrochelate bearing ditopic carboxylic acid ligands and lateral butyl groups affording readily stable crystalline MOFs at low modulator concentration and exhibiting high BET surface area reaching up to 650 m^2 g^{-1} after supercritical CO_2 ($ScCO_2$) activation from acetonitrile

Materials Synthesis and Characterization

Materials: All reagents were obtained from commercial sources and used without further purification, unless otherwise noted.

[a] *Department of Mathematics and Natural Sciences, Gulf University for Science and Technology, Kuwait*
[b] *Functional Materials Group, Gulf University for Science and Technology, Kuwait*
[c] *Department of Chemistry and International Institute for Nanotechnology, Northwestern University, 2145 Sheridan Road, Evanston, Illinois 60208, United States*
[d] *Department of Chemical & Biological Engineering, Northwestern University, Evanston, Illinois 60208, United States*
[⊥] S.S and K.B.I contributed equally to this work
Electronic Supplementary Information (ESI) available: [Figures S1: (Experimental PXRD patterns of Zr-GU-3,4); Figures S2: (Obtained crystal for Zr-GU-2 for SCXRD analysis); Figures S3: (comparative experimental PXRD patterns of Zr-GU-1 synthesized, after $ScCO_2$ activation and DMF soaked post activation); Table S1 (Crystal data and structure refinement for Zr-GU-1)]. See DOI: 10.1039/x0xx00000x

X-Ray Diffraction Analyses: Powder X-ray diffraction (PXRD) of MOFs were measured at room temperature on a STOE-STADI MP powder diffractometer equipped with an asymmetric curved Germanium monochromator (CuKα1 radiation, λ = 1.54056 Å) and one-dimensional silicon strip detector (MYTHEN2 1K from DECTRIS). The line focused Cu X-ray tube was operated at 40 kV and 40 mA. The activated powder was sandwiched between two Kapton foils and measured in transmission geometry in a rotating holder. Intensity data from 1 to 40 degrees two theta were collected.

N_2 Sorption Measurements: N_2 adsorption and desorption isotherms on activated materials were measured at Northwestern University on an ASAP 2420 (Micromeritics) instrument at 77 K after activation. Ultra-high purity N_2 (99.999%) was purchased from Airgas and used as received. Sorption measurements were carried out on approximately 30-40 mg of sample.

Supercritical CO_2 ($ScCO_2$) procedure: Supercritical CO_2 activation experiments were performed on Tousimis Samdri PVT-30 critical point dryer. Before doing the $ScCO_2$ drying, the as synthesized materials were soaked in DMF for 3 days followed by solvent exchange into ethanol, acetonitrile~~, or perfluoropentane~~ **for 1 day. The solvent was refreshed every 12 h, and 12 mL of fresh solvent was added into the vials. The material was then transferred to a small glass container with minimal solvent to cover the sample for $ScCO_2$ drying (Note: do not let the materials dry in solvent, and make sure the materials are always submerged in solvent before applying $ScCO_2$ drying procedure).**

Single-Crystal X-ray Diffraction: SCXRD data was collected at 200 K, using a Rigaku Cu-Synergy diffractometer equipped with shutterless electronic-noise free Hybrid Photon Counting (HPC) detector and Cryostream 80-500K (Cryostream Oxford Cryosystems, Oxford, United Kingdom), CuKα (λ = 1.54184 Å) microfocus source with a beam size of ~110 µm and a 4-circle Kappa geometry goniometer. The single crystals were mounted on MicroMesh (MiTeGen) with paratone oil. The structures were determined by intrinsic phasing (SHELXT 2018/2) and refined by full-matrix least-squares refinement (SHELXL-2018/3) using the Olex2 software packages. The disordered non-coordinated solvents and alkane side chains were removed using the solvent marks option in Olex2 software. The refinement results are summarized in Table S1. Crystallographic data for the Zr-GU-1 in CIF format have been deposited in the Cambridge Crystallographic Data Centre (CCDC) under deposition number 2224952.

Synthesis of Zr-Clathrochelate MOF (Zr-GU-1): Zr-GU-1 MOF was prepared solvothermally by combining a mixture of Clathrochelate linker GU-1 (0.0129 mmol, 11.9 mg) and $ZrOCl_2.8H_2O$ (0.0155 mmol, 5.0 mg) in 1 mL DMF and 20 µL TFA at 120°C for 48 h. The crystals were collected and washed three times over two days with anhydrous DMF and then sequentially immersed in anhydrous DMF.

Results and Discussion

Previous reports have shown the synthesis of clathrochelate-based MOFs using copper or zinc metal nodes[6,42,43], however, to the best of our knowledge, no crystal structures have been reported for iron (II) clathrochelate-based MOFs using zirconium nodes. Therefore, we attempted to synthesize these latter and obtain their single crystal structures by employing the iron (II) clathrochelate dicarboxylic acid linkers GU-1 to -4, shown in scheme 1 below, which were synthesized following a procedure reported in the literature[42] and that bear different lateral groups, namely, butyl, cyclohexyl, phenyl and methyl moieties. Zr-GU-1 MOF was synthesized solvothermally by mixing 12.9 µmol of GU-1 (linker with soluble butyl chain) and $ZrOCl_2.8H_2O$ (15.5 µmol) in 1 mL of DMF and 20 µL of TFA at 120°C for 48 h. Similar conditions were used to prepare the Zr-clathrochelate MOFs Zr-GU-2 to -4 which bear various lateral chains on the linker (R = cyclohexyl, phenyl, or methyl). Although the MOF synthesis using the abovementioned linkers (GU-2 to -4) seems feasible, their lower solubility compared to GU-1 required some additional fine-tuning to obtain a crystalline sample of better quality (Figure 2).

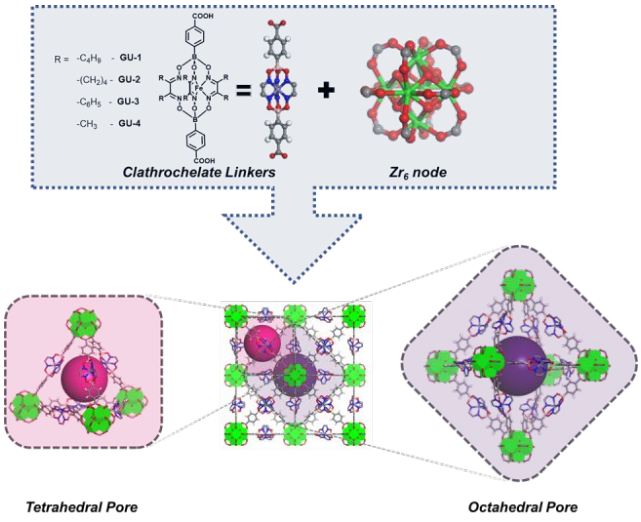

Scheme 1. Synthetic scheme of Zr-clathrochelate MOFs Zr-GU-1 to -4 and formation of octahedral and tetrahedral cavities within the framework.

Interestingly, stable single crystals of Zr-GU-1 with suitable sizes for SCXRD analysis were obtained by employing the synthetic condition mentioned above. SCXRD data analysis revealed the atomic structure of Zr-GU-1 which crystallizes in the *Fm-3m* space group with an fcu topology (Figure 1) with lattice constants $a = b = c = 37.5848(3)$ Å and $\alpha = \beta = \gamma = 90°$. Zr-GU-1 is composed of hexanuclear zirconium (Zr_6) clusters

bridged by ditopic iron (II) clathrochelate ligands to form both octahedral and tetrahedral cavities connected by triangular windows/pore apertures (Scheme 1). As it could be noticed from Figure 2, the as-synthesized and simulated powder X-ray diffraction (PXRD) patterns of Zr-GU-1 are well-matched, thus, confirming the phase purity of the bulk sample.

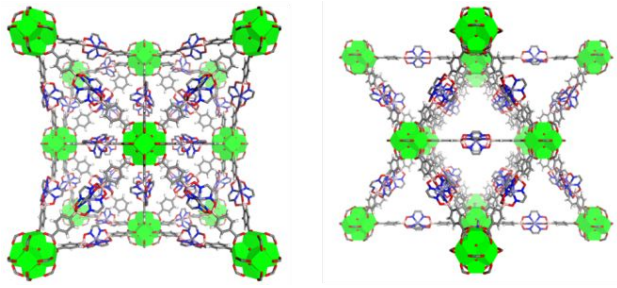

Figure 1. SCXRD structure for Zr-GU-1 along the a and b-axis. Hydrogen atoms and disordered linkers are removed for clarity.

Several attempts were carried out to obtain SCXRD structures for the remaining MOFs Zr-GU-2 to -4. First, in order to overcome the low solubility of the clathrochelate linkers GU-2- to -4, we attempted a solvothermal synthesis of Zr-GU-2 to -4 under the same conditions described above to make Zr-GU-1 but employing a lower linker concentration of 2.9 µmol mmol instead of 12.9 µmol. These conditions were successful affording large single crystals of Zr-GU-2 but whose SCXRD structure was not feasible because the crystals decomposed soon after removal of the solvent (Figure S2). Further efforts to obtain single crystals of Zr-GU-3 and Zr-GU-4 using other modulators such as acetic acid or formic acid were unsuccessful and increasing the amount of the modulator resulted in the formation of different products as confirmed by PXRD analysis (Figure S1).

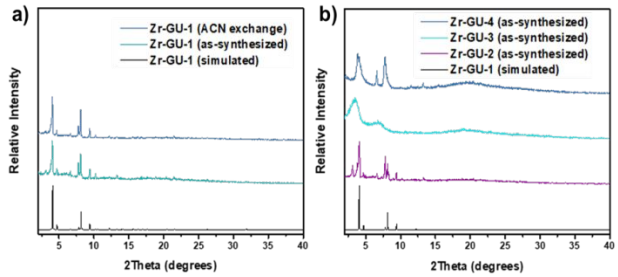

Figure 2. a) Experimental and simulated PXRD patterns of Zr-GU-1 as-synthesized and following ACN exchange. b) Comparison of experimental PXRD patterns of Zr-GU-2 to -4 with simulated PXRD pattern of Zr-GU-1.

To probe the porosity of Zr-GU-1, we first tried thermal activation at 100°C, but N_2 adsorption isotherm at 77K revealed no porosity. Therefore, an alternative attempt has been carried out by using supercritical CO_2 activation ($ScCO_2$) of Zr-GU-1 from either ethanol (EtOH) or acetonitrile (ACN) where the latter portrayed the highest porosity obtained for Zr-GU-1 compared to other activation methods with an experimental total pore volume of 0.37 $cm^3\ g^{-1}$ at $P/P^0 = 0.9$ compared to the theoretical pore volume of 0.83 $cm^3\ g^{-1}$. The apparent Brunauer–Emmett–Teller (BET) surface area of Zr-GU-1 was found to be 650 $m^2\ g^{-1}$ (Figure 3). It is noteworthy that the crystallinity of Zr-GU-1 was lost following $ScCO_2$ activation but was partially restored after soaking it back in ACN (Figure S3), therefore, indicating a reversible structural change between an 'open' and 'closed' form and which could be attributed to the lower experimental pore volume.

Due to the relatively high crystallinity of Zr-GU-2 compared to Zr-GU-3 and Zr-GU-4, we further investigated its bulk porosity using N_2 adsorption isotherms. Interestingly, Zr-GU-2 exhibits significantly higher BET surface areas after thermal activation at 100°C and $ScCO_2$ from ACN compared to that of Zr-GU-1. The BET surface was found to be 475 $m^2\ g^{-1}$ after thermal activation compared to the negligible BET surface area for Zr-GU-1 when using the same activation technique. Furthermore, $ScCO_2$ activation after ACN exchange yielded a BET surface area of 850 $m^2\ g^{-1}$ with a pore volume of 0.49 $cm^3\ g^{-1}$ (Figure 3) compared to the theoretical pore volume of 0.91 $cm^3\ g^{-1}$. This larger BET surface area could mainly be attributed to the bulkier cyclohexyl lateral groups in Zr-GU-2 which are positioned in close proximity to the framework walls, thus, allowing the structure to maintain its 'open' form as opposed to the linear butyl groups in Zr-GU-1.

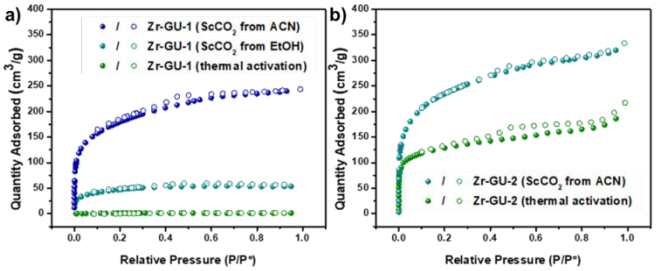

Figure 3. Experimental N_2 adsorption and desorption isotherms at 77K after $ScCO_2$ and thermal activation for a) Zr-GU-1 and b) Zr-GU-2.

Conclusions

In summary, new metal organic frameworks (MOFs) based on zirconium were successfully made using iron (II) clathrochelate-bearing ditopic carboxylic acid ligands and Zr_6 inorganic nodes. The stable crystalline MOFs were obtained from the iron (II) clathrochelate based dicarboxylic acid linkers bearing lateral butyl groups **Zr-GU-1** and its formation was confirmed by single-crystal X-ray crystallography. N_2-adsorption study of **Zr-GU-1** portrays porous nature with pore volume of 0.37 $cm^3\ g^{-1}$. Furthermore, the apparent Brunauer–Emmett–Teller (BET) surface area of **Zr-GU-1** was found to be

650 m^2 g^{-1} after acetonitrile $ScCO_2$ activation. Additionally, replacing the butyl groups with bulkier cyclohexyl groups allowed the framework to achieve a BET surface area of 850 m^2 g^{-1}.

Author Contributions

"Conceptualization, B.A. and O.F.; methodology, B.A. and O.F.; software, S.S., K.I., and H.X.; validation, H.X., Y.Y. and Z.Z.; formal analysis, B.A. and O.F; investigation, S.S., K.I., and H.X.; resources, B.A. and O.F.; writing—original draft preparation, X.X.; writing—review and editing, S.S., K.I., H.X., B.A. and O.F.; visualization, X.X.; supervision, B.A. and O.F; project administration, B.A. and O.F.; funding acquisition, B.A. and O.F. All authors have read and agreed to the published version of the manuscript."

Conflicts of interest

"There are no conflicts to declare".

Acknowledgements

B.A. would like to thank the Kuwait Foundation for the Advancement of Sciences (KFAS, project number: PN18-14SC-01) for partially supporting this work. O.K.F. acknowledges the support from the U.S. Department of Energy (DOE) Office of Science, Basic Energy Sciences Program for separation (DE-FG02-08ER15967). This work made use of the EPIC facility of Northwestern University's NUANCE Center, which has received support from the Soft and Hybrid Nanotechnology Experimental (SHyNE) Resource (NSF ECCS-1542205); the MRSEC program (NSF DMR-1720139) at the Materials Research Center; the International Institute for Nanotechnology (IIN); the Keck Foundation; and the State of Illinois, through the IIN. This work made use of the IMSERC at Northwestern University, which has received support from the Soft and Hybrid Nanotechnology Experimental (SHyNE) Resource (NSF ECCS-1542205), the State of Illinois, and the International Institute for Nanotechnology (IIN).

Notes and references

1 Chen, F.; F., D.H.; Liang, F.; A., P.J.; Kun-Yu, W.; Tian-Hao, Y.; Hong-Cai, Z. Metal–Organic Frameworks as Versatile Platforms for Organometallic Chemistry. Inorganics 2021, 9, 27, doi:10.3390/inorganics9040027.

2 Jiao, L.; Seow, J.Y.R.; Skinner, W.S.; Wang, Z.U.; Jiang, H.-L. Metal–organic frameworks: Structures and functional applications. Materials Today 2019, 27, 43-68, doi:https://doi.org/10.1016/j.mattod.2018.10.038.

3 Unnikrishnan, V.; Zabihi, O.; Ahmadi, M.; Li, Q.; Blanchard, P.; Kiziltas, A.; Naebe, M. Metal–organic framework structure–property relationships for high-performance multifunctional polymer nanocomposite applications. Journal of Materials Chemistry A 2021, 9, 4348-4378, doi:10.1039/D0TA11255K.

4 Ye, X.; Liu, D. Metal–Organic Framework UiO-68 and Its Derivatives with Sufficiently Good Properties and Performance Show Promising Prospects in Potential Industrial Applications. Crystal Growth & Design 2021, 21, 4780-4804, doi:10.1021/acs.cgd.1c00460.

5 Chakraborty, G.; Park, I.-H.; Medishetty, R.; Vittal, J.J. Two-Dimensional Metal-Organic Framework Materials: Synthesis, Structures, Properties and Applications. Chemical Reviews 2021, 121, 3751-3891, doi:10.1021/acs.chemrev.0c01049.

6 Gong, W.; Xie, Y.; Pham, T.D.; Shetty, S.; Son, F.A.; Idrees, K.B.; Chen, Z.; Xie, H.; Liu, Y.; Snurr, R.Q.; et al. Creating Optimal Pockets in a Clathrochelate-Based Metal–Organic Framework for Gas Adsorption and Separation: Experimental and Computational Studies. Journal of the American Chemical Society 2022, 144, 3737-3745, doi:10.1021/jacs.2c00011.

7 Jiang, C.; Wang, X.; Ouyang, Y.; Lu, K.; Jiang, W.; Xu, H.; Wei, X.; Wang, Z.; Dai, F.; Sun, D. Recent advances in metal–organic frameworks for gas adsorption/separation. Nanoscale Advances 2022, 4, 2077-2089, doi:10.1039/D2NA00061J.

8 Ma, Z.L.; Liu, P.X.; Liu, Z.Y.; Wang, J.J.; Li, L.B.; Tian, L. A Thermally and Chemically Stable Copper(II) Metal–Organic Framework with High Performance for Gas Adsorption and Separation. Inorganic Chemistry 2021, 60, 6550-6558, doi:10.1021/acs.inorgchem.1c00357.

9 Wang, H.; Mahle, J.J.; Tovar, T.M.; Peterson, G.W.; Hall, M.G.; DeCoste, J.B.; Buchanan, J.H.; Karwacki, C.J. Solid-Phase Detoxification of Chemical Warfare Agents using Zirconium-Based Metal Organic Frameworks and the Moisture Effects: Analyze via Digestion. ACS Applied Materials & Interfaces 2019, 11, 21109-21116, doi:10.1021/acsami.9b04927.

10 Yin, H.-Q.; Yin, X.-B. Metal–Organic Frameworks with Multiple Luminescence Emissions: Designs and Applications. Accounts of Chemical Research 2020, 53, 485-495, doi:10.1021/acs.accounts.9b00575.

11 Bhattacharya, S.; Ayass, W.W.; Taffa, D.H.; Nisar, T.; Balster, T.; Hartwig, A.; Wagner, V.; Wark, M.; Kortz, U. Polyoxopalladate-Loaded Metal–Organic Framework (POP@MOF): Synthesis and Heterogeneous Catalysis. Inorganic Chemistry 2020, 59, 10512-10521, doi:10.1021/acs.inorgchem.0c00875.

12 Yang, D.; Gates, B. Catalysis by Metal Organic Frameworks: Perspective and Suggestions for Future Research. ACS Catalysis 2019, 9, doi:10.1021/acscatal.8b04515.

13 Rambabu, D.; Lakraychi, A.E.; Wang, J.; Sieuw, L.; Gupta, D.; Apostol, P.; Chanteux, G.; Goossens, T.; Robeyns, K.; Vlad, A. An Electrically Conducting Li-Ion Metal–Organic Framework. Journal of the American Chemical Society 2021, 143, 11641-11650, doi:10.1021/jacs.1c04591.

14 Jiang, Y.; Zhao, H.; Yue, L.; Liang, J.; Li, T.; Liu, Q.; Luo, Y.; Kong, X.; Lu, S.; Shi, X.; et al. Recent advances in lithium-based batteries using metal organic frameworks as electrode materials. Electrochemistry Communications 2021, 122, 106881, doi:https://doi.org/10.1016/j.elecom.2020.106881.

15 Liu, X.; Shan, Y.; Zhang, S.; Kong, Q.; Pang, H. Application of metal organic framework in wastewater treatment. Green Energy & Environment 2022, doi:https://doi.org/10.1016/j.gee.2022.03.005.

16 Chen, X.; Zhuang, Y.; Rampal, N.; Hewitt, R.; Divitini, G.; O'Keefe, C.; Liu, X.; Whitaker, D.; Wills, J.; Jugdaohsingh, R.; et al. Formulation of Metal–Organic Framework-Based Drug Carriers by Controlled Coordination of Methoxy PEG Phosphate: Boosting Colloidal Stability and Redispersibility. Journal of the American Chemical Society 2021, 143, 13557–13572, doi:10.1021/jacs.1c03943.

17 Gu, J.-Z.; Wen, M.; Liang, X.; Shi, Z.; Kirillova, M.; Kirillov, A. Multifunctional Aromatic Carboxylic Acids as Versatile

Building Blocks for Hydrothermal Design of Coordination Polymers. Crystals 2018, 8, 83, doi:10.3390/cryst8020083.
18 Ahamad, M.N.; Khan, M.S.; Shahid, M.; Ahmad, M. Metal organic frameworks decorated with free carboxylic acid groups: topology, metal capture and dye adsorption properties. Dalton Transactions 2020, 49, 14690-14705, doi:10.1039/D0DT02949A.
19 Gu, J.; Wen, M.; Liang, X.; Shi, Z.; Kirillova, M.V.; Kirillov, A.M. Multifunctional Aromatic Carboxylic Acids as Versatile Building Blocks for Hydrothermal Design of Coordination Polymers. Crystals 2018, 8, doi:10.3390/cryst8020083.
20 Karmakar, A.; Goldberg, I. Coordination polymers of flexible tetracarboxylic acids with metal ions. I. Synthesis of CH2- and (CH2)2-spaced bis(oxy)isophthalic acid ligands, and structural characterization of their polymeric adducts with lanthanoid ions. CrystEngComm 2011, 13, 339-349, doi:10.1039/C0CE00474J.
21 Alezi, D.; Jia, J.; Bhatt, P.M.; Shkurenko, A.; Solovyeva, V.; Chen, Z.; Belmabkhout, Y.; Eddaoudi, M. Reticular Chemistry for the Construction of Highly Porous Aluminum-Based nia-Metal–Organic Frameworks. Inorganic Chemistry 2022, 61, 10661-10666, doi:10.1021/acs.inorgchem.2c00756.
22 He, T.; Kong, X.-J.; Zhou, J.; Zhao, C.; Wang, K.; Wu, X.-Q.; Lv, X.-L.; Si, G.-R.; Li, J.-R.; Nie, Z.-R. A Practice of Reticular Chemistry: Construction of a Robust Mesoporous Palladium Metal–Organic Framework via Metal Metathesis. Journal of the American Chemical Society 2021, 143, 9901-9911, doi:10.1021/jacs.1c04077.
23 Wuttke, S. Introduction to Reticular Chemistry. Metal–Organic Frameworks and Covalent Organic Frameworks By Omar M. Yaghi, Markus J. Kalmutzki, and Christian S. Diercks. Angewandte Chemie International Edition 2019, 58, 14024-14024, doi:https://doi.org/10.1002/anie.201906230.
24 Gropp, C.; Canossa, S.; Wuttke, S.; Gándara, F.; Li, Q.; Gagliardi, L.; Yaghi, O.M. Standard Practices of Reticular Chemistry. ACS Central Science 2020, 6, 1255-1273, doi:10.1021/acscentsci.0c00592.
25 Guillerm, V.; Eddaoudi, M. The Importance of Highly Connected Building Units in Reticular Chemistry: Thoughtful Design of Metal–Organic Frameworks. Accounts of Chemical Research 2021, 54, 3298-3312, doi:10.1021/acs.accounts.1c00214.
26 Chen, P.; He, X.; Pang, M.; Dong, X.; Zhao, S.; Zhang, W. Iodine Capture Using Zr-Based Metal–Organic Frameworks (Zr-MOFs): Adsorption Performance and Mechanism. ACS Applied Materials & Interfaces 2020, 12, 20429-20439, doi:10.1021/acsami.0c02129.
27 Kim, H.; Kim, D.; Moon, D.; Choi, Y.N.; Baek, S.B.; Lah, M.S. Symmetry-guided syntheses of mixed-linker Zr metal–organic frameworks with precise linker locations. Chemical Science 2019, 10, 5801-5806, doi:10.1039/C9SC01301F.
28 Ardila-Suárez, C.; Rodríguez-Pereira, J.; Baldovino-Medrano, V.G.; Ramírez-Caballero, G.E. An analysis of the effect of zirconium precursors of MOF-808 on its thermal stability, and structural and surface properties. CrystEngComm 2019, 21, 1407-1415, doi:10.1039/C8CE01722K.
29 Mieno, H.; Kabe, R.; Allendorf, M.D.; Adachi, C. Thermally activated delayed fluorescence of a Zr-based metal–organic framework. Chemical Communications 2018, 54, 631-634, doi:10.1039/C7CC08595H.
30 Xiao, F.; Hu, X.; Chen, Y.; Zhang, Y. Porous Zr-Based Metal-Organic Frameworks (Zr-MOFs)-Incorporated Thin-Film Nanocomposite Membrane toward Enhanced Desalination Performance. ACS Applied Materials & Interfaces 2019, 11, 47390-47403, doi:10.1021/acsami.9b17212.
31 Furukawa, H.; Gándara, F.; Zhang, Y.-B.; Jiang, J.; Queen, W.L.; Hudson, M.R.; Yaghi, O.M. Water Adsorption in Porous Metal–Organic Frameworks and Related Materials. Journal of the American Chemical Society 2014, 136, 4369-4381, doi:10.1021/ja500330a.
32 Cavka, J.H.; Jakobsen, S.; Olsbye, U.; Guillou, N.; Lamberti, C.; Bordiga, S.; Lillerud, K.P. A New Zirconium Inorganic Building Brick Forming Metal Organic Frameworks with Exceptional Stability. Journal of the American Chemical Society 2008, 130, 13850-13851, doi:10.1021/ja8057953.
33 Bai, Y.; Dou, Y.; Xie, L.-H.; Rutledge, W.; Li, J.-R.; Zhou, H.-C. Zr-based metal–organic frameworks: design, synthesis, structure, and applications. Chemical Society Reviews 2016, 45, 2327-2367, doi:10.1039/C5CS00837A.
34 Gao, X.; Guo, B.; Guo, C.; Meng, Q.; Liang, J.; Liu, J. Zirconium-Based Metal–Organic Framework for Efficient Photocatalytic Reduction of CO2 to CO: The Influence of Doped Metal Ions. ACS Applied Materials & Interfaces 2020, 12, 24059-24065, doi:10.1021/acsami.0c05631.
35 Qiao, G.-Y.; Yuan, S.; Pang, J.; Rao, H.; Lollar, C.T.; Dang, D.; Qin, J.-S.; Zhou, H.-C.; Yu, J. Functionalization of Zirconium-Based Metal–Organic Layers with Tailored Pore Environments for Heterogeneous Catalysis. Angewandte Chemie International Edition 2020, 59, 18224-18228, doi:https://doi.org/10.1002/anie.202007781.
36 Zheng, J.; Wu, M.; Jiang, F.; Su, W.; Hong, M. Stable porphyrin Zr and Hf metal–organic frameworks featuring 2.5 nm cages: high surface areas, SCSC transformations and catalyses. Chemical Science 2015, 6, 3466-3470, doi:10.1039/C5SC00213C.
37 Tang, J.; Li, P.; Islamoglu, T.; Li, S.; Zhang, X.; Son, F.A.; Chen, Z.; Mian, M.R.; Lee, S.-J.; Wu, J.; et al. Micropore environment regulation of zirconium MOFs for instantaneous hydrolysis of an organophosphorus chemical. Cell Reports Physical Science 2021, 2, 100612, doi:https://doi.org/10.1016/j.xcrp.2021.100612.
38 Ma, K.; Wasson, M.C.; Wang, X.; Zhang, X.; Idrees, K.B.; Chen, Z.; Wu, Y.; Lee, S.-J.; Cao, R.; Chen, Y.; et al. Near-instantaneous catalytic hydrolysis of organophosphorus nerve agents with zirconium-based MOF/hydrogel composites. Chem Catalysis 2021, 1, 721-733, doi:https://doi.org/10.1016/j.checat.2021.06.008.
39 Liu, Y.; Howarth, A.J.; Vermeulen, N.A.; Moon, S.-Y.; Hupp, J.T.; Farha, O.K. Catalytic degradation of chemical warfare agents and their simulants by metal-organic frameworks. Coordination Chemistry Reviews 2017, 346, 101-111, doi:https://doi.org/10.1016/j.ccr.2016.11.008.
40 Wang, J.-X.; Yin, J.; Shekhah, O.; Bakr, O.M.; Eddaoudi, M.; Mohammed, O.F. Energy Transfer in Metal–Organic Frameworks for Fluorescence Sensing. ACS Applied Materials & Interfaces 2022, 14, 9970-9986, doi:10.1021/acsami.1c24759.
41 Plonka, A.M.; Wang, Q.; Gordon, W.O.; Balboa, A.; Troya, D.; Guo, W.; Sharp, C.H.; Senanayake, S.D.; Morris, J.R.; Hill, C.L.; et al. In Situ Probes of Capture and Decomposition of Chemical Warfare Agent Simulants by Zr-Based Metal Organic Frameworks. Journal of the American Chemical Society 2017, 139, 599-602, doi:10.1021/jacs.6b11373.
42 Chen, Z.; Idrees, K.B.; Shetty, S.; Xie, H.; Wasson, M.C.; Gong, W.; Zhang, X.; Alameddine, B.; Farha, O.K. Regulation of Catenation in Metal–Organic Frameworks with Tunable Clathrochelate-Based Building Blocks. Crystal Growth & Design 2021, 21, 6665-6670, doi:10.1021/acs.cgd.1c01151.
43 Marmier, M.; Wise, M.D.; Holstein, J.J.; Pattison, P.; Schenk, K.; Solari, E.; Scopelliti, R.; Severin, K. Carboxylic Acid Functionalized Clathrochelate Complexes: Large, Robust, and Easy-to-Access Metalloligands. Inorganic Chemistry 2016, 55, 4006-4015, doi:10.1021/acs.inorgchem.6b00276.